UCRL-95567 Rev 1
PREPRINT

UCRL--95567-Rev.1

DE87 002380

TMX-U TANDEM-MIRROR THERMAL-BARRIER EXPERIMENTS

T. C. Simonen, S. L. Allen, D. E. Baldwin, J. D. Barter, L. V. Berzins, M. R. Carter, T. A. Casper, J. F. Clauser, F. H. Coensgen, D. L. Correll, W. F. Cummins, C. C. Damm, G. Dimonte, B. H. Failor, S. Falabella, J. H. Foote, A. H. Futch, R. K. Goodman, D. P. Grubb, D. N. Hill, E. B. Hooper, R. S. Hornady, R. D. Horton, W. L. Hsu, B. Huff, A. L. Hunt, R. A. James, C. J. Lasnier, C. A. Leavitt, W. H. Meyer, J. M. Moller, A. W. Molvik, W. E. Nexsen, D. E. Perkins, W. L. Pickles, P. A. Pincosy, G. D. Porter, P. Poulsen, D. B. Ress, M. Shiho, E. H. Silver, B. W. Stallard, W. C. Turner, R. D. Wood, and T. L. Yu

This paper was prepared for submittal to the Proceedings of the Eleventh International Conference on Plasma Physics and Controlled Nuclear Fusion Research, Kyoto, Japan, November 13-20, 1986

October 29, 1986

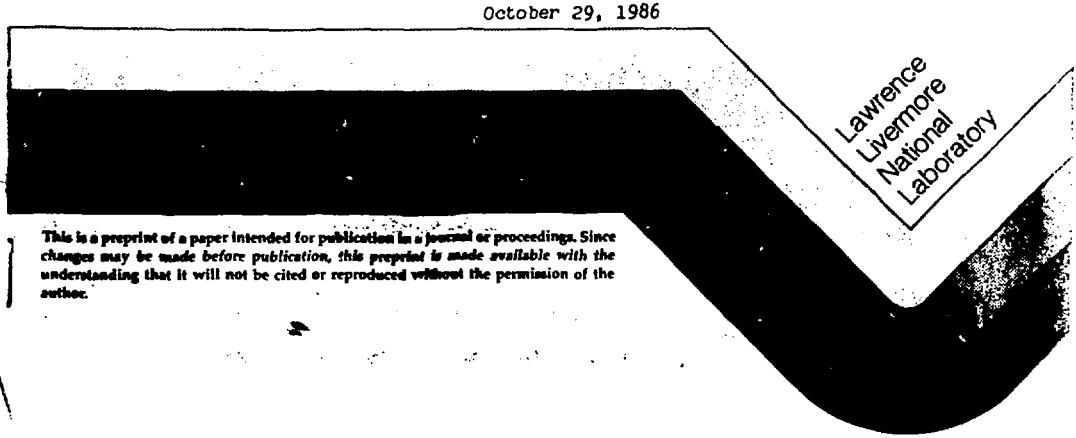

TMX-U TANDEM-MIRROR THERMAL-BARRIER EXPERIMENTS*

T. C. Simonen, S. L. Allen, D. E. Baldwin, J. D. Barter,**
L. V. Berzins,*** M. R. Carter,*** T. A. Casper, J. F. Clauser,
F. H. Coensgen, D. L. Correll, W. F. Cummins, C. C. Damm,
G. Dimonte,** B. H. Failor,*** S. Falabella,*** J. H. Foote,
A. H. Futch, R. K. Goodman, D. P. Grubb, D. N. Hill,
E. B. Hooper, R. S. Hornady, R. D. Horton,** W. L. Hsu,****
B. Huff,** A. L. Hunt, R. A. James, C. J. Lasnier,†
C. A. Leavitt,** W. H. Meyer, J. M. Moller, A. W. Molvik,
W. E. Nexsen, D. E. Perkins, W. L. Pickles, P. A. Pincosy,**
G. D. Porter, P. Poulsen, D. B. Ress, M. Shiho,†† E. H. Silver,
B. W. Stallard, W. C. Turner, R. D. Wood, and T. L. Yu†††
Lawrence Livermore National Laboratory, University of California
Livermore, CA 94550

*Work performed under the auspices of the U.S. Department of Energy by the Lawrence Livermore National Laboratory under contract number W-7405-ENG-48.

**TRW Corp., Redondo Beach, CA

***University of California, Davis, CA

****Sandia National Laboratory, Livermore, CA

†University of Maryland, College Park, MD

††Japan Atomic Energy Research Institute, Tohai, Naka, Ibaraki

†††Johns Hopkins University, Baltimore, MD

TMX-U TANDEM-MIRROR THERMAL-BARRIER EXPERIMENTS

ABSTRACT

Thermal-barrier experiments have been carried out in the Tandem Mirror Experiment-Upgrade (TMX-U). Measurements of nonambipolar and ambipolar radial transport show that these transport processes, as well as end losses, can be controlled at modest densities and durations. Central-cell heating methods using ion-cyclotron heating (ICH) and neutral-beam injection have been demonstrated. Potential measurements with recently developed methods indicate that deep thermal barriers can be established.

1. *INTRODUCTION*

This paper describes thermal-barrier experiments from the Tandem Mirror Experiment-Upgrade (TMX-U) using new heating systems and improved diagnostics aimed at improving our understanding of how tandem mirrors work. We can operate TMX-U as a standard tandem mirror at densities near 10^{13} cm^{-3} and ion temperatures of 2 keV with 4 ms energy confinement time. However, we have concentrated our experiments on the thermal-barrier mode which could scale to a reactor. In this mode, three processes limit the central-cell density. First is nonambipolar radial transport, second is ambipolar transport, and third is the loss of end plugging. When those three loss processes are controlled, the central-cell density increases at the ionization rate up to a maximum line averaged value of 1 to 3 × 10^{12} cm^{-3}.

The purpose of the program of measurements presented here has been to improve our understanding of the above three processes in order to continue increasing the density toward the $10^{13} cm^{-3}$ theoretical maximum. Because of changes in funding priorities, for the present we will not be able to complete this program on TMX-U, but the work will be continued on the other tandem mirror facilities elsewhere such as GAMMA-10, TARA, and Phaedrus. However, we have made considerable progress, especially in understanding and controlling radial transport, which was of considerable concern in the past. Section 2 describes this work. The remaining sections deal with two topics related to understanding and controlling end losses. Section 3 summarizes our progress on central-cell heating and fueling by ICH and neutral beams, which ultimately control barrier filling. Section 4 describes our recent measurements of thermal-barrier axial potential profiles.

TMX-U employs minimum-B, thermal-barrier end-plugs [1,2]. The 0.3-T nonaxisymmetric central cell is 8 m long, and is currently operated with a 24-cm radius limiter. The heating systems operate for a 75-ms duration. Ten of the 24 neutral injectors are located in the central cell and operate at either 2 or 20 kV. A total of fourteen 20-kV beams are used in the end plug as sloshing beams (47° and 40°) and as pump beams (18° and 24°). Two 200-kW, 28-GHz gyrotrons are used in each end cell. Two 200-kW transmitters drive separate ICH antennas at each end of the central cell, between which D_2 gas is injected to provide

fueling. The end-wall plasma potential control (PPC) plates [3] can operate either grounded or floating.

2. RADIAL TRANSPORT AND PARTICLE ACCOUNTABILITY

In TMX-U, nonambipolar radial transport is driven by the central-cell potential [4]. Recent experiments with grounded end walls indicate that the nonambipolar radial current depends on the plug sloshing beam current in addition to the plasma potential. (The two terms are comparable.) A portion of the sloshing ion loss is radial. To compare the central-cell transport with resonant neoclassical theory, we evaluate its nonambipolar confinement time by using regression analysis to subtract the inferred radial sloshing ion current from the total measured net current. In Fig. 1a, the variation of $\tau_{\perp NA}^{cc}$ with potential is compared with the theoretical prediction at $r = 20$ cm assuming $T_{ic} \sim \phi/4$. Good agreement is found in this radially averaged confinement time.

Nonambipolar transport has been significantly decreased by electrically floating segmented end PPC plates [3]. During plasma operation, the 26 plates on each end charge to a negative poential of 1- to 3-kV negative through 10^4 ohm resistors to grounds. Potential measurements have now demonstrated that the end-wall plates reduce the central-cell plasma potential, confirming the conclusion deduced from the effect of the plates on the nonambipolar radial ion transport [1,3]. Figure 1b shows the time history of the central-cell potential during a discharge in which the plates were floated during plugging. The potential on-axis dropped from 1.1 to 0.5 kV with the plates floating. The plates usually drop twice as much below ground. In this shot, plugging failed 3 ms later and the potential partially recovered.

Since radial transport can occur independently in the central cell and the end cells, a low PPC plate net current does not guarantee small nonambipolar radial transport in the central cell. Nor does it indicate low ambipolar transport. Consequently, particle accountability is used to evaluate the amount of ambipolar radial transport in the plasma; here we consider the core of the plasma ($r < 10$ cm). The ion particle balance equation is:

$$\frac{qdN}{dt} = I_s - I_{\parallel} - I_{\perp}^{NA} - I_{\perp}^{A}$$

where I_s is the core ionization source current determined from an absolutely calibrated imaging high-speed H-alpha camera system [5], $I_{\parallel}$ is the axial ion loss current obtained from an array of Faraday cups, $I_{\perp}^{NA}$ is the nonambipolar loss current measured by the end-wall PPC plates, and $I_{\perp}^{A}$ is the residual (ambipolar) current required to balance the equation. Results of our measurements are shown in Fig. 2, which shows (a) the central-cell density and (b) a comparison between the measured core source I_s and the sum of the terms: $I_T = (qdN/dt + I_{\perp}^{NA} + I_{\parallel})$. Between 25 to 30 ms we have achieved plasma conditions with small axial losses and the PPC plates were floated

(10^4 ohms) to reduce nonambipolar radial losses. The total particle-confinement time under these conditions is 10 ms. During this plugged period (25-30 ms) the density rises and is the main contribution to I_T. Later in this shot, we observe a discrepancy indicative of some ambipolar transport, which is reduced when the $2\omega_{ce}$ electron-cyclotron heating (ECH) is turned off. Under usual operating conditions, I_s and I_T agree to better than a factor of two, implying that ambipolar losses are no greater than the sum of the other losses. However, under some conditions of central-cell fueling and heating rates, we observe larger amounts of ambipolar transport usually accompanied by 2- to 7-kHz fluctuations.

Figure 3 shows the central-cell radial "density" (thallium ionization current) and potential profiles with and without significant ambipolar radial transport. At 22 ms, the measured (H-alpha) ambipolar transport is large and the radial "density" profile is flat. During this time the axial ion end losses are plugged and the radial potential profile is peaked. Later, at 42 ms, the measured ambipolar radial transport is small and the "density" profile is strongly peaked. At this time axial plugging is weak and the potential profile is nearly constant in the plasma core. Such peaked density profiles are also measured during plugging, when the central-cell density increases.

3. CENTRAL-CELL HEATING AND FUELING

End plugging requires that the passing-ion thermal-barrier collisional filling rate be reduced below the pumping rate. The filling rate should be reduced by ICH of the passing ions and by reducing the passing-ion density at the plug mirrors through anisotropic trapping in the central cell. Our previous experiments used gas fueling 2.25 m west of the central-cell midplane, and a double half-turn loop 1.26 m west of the midplane. These resulted in efficient perpendicular heating of mirror-trapped ions to 2 keV but did not heat ions entering the west plug. Present experiments use a more symmetrical arrangement, with gas fueling near the central-cell midplane (0.25 m east) and double half-turn antennas toward both ends of the central cell. The ICH frequencies are selected for resonance between each antenna and the gas box so that newly ionized particles must pass through an ICH resonance before reaching an end cell. The increase in the parallel ion temperature with ICH power is similar at both ends, as shown in Fig. 4a. Using this ICH configuration, we increased the central-cell density to 3×10^{12} cm^{-3} as shown in Fig. 4b. In this shot, $T_{ec} = 90$ eV and $T_{ic} \approx 160$ eV. During this operation, we achieved long axial and nonambipolar confinement times; however, low-frequency fluctuations driven by the ICH limited the ambipolar confinement time to 2 ms.

With 20-kV extraction voltage, the ten central-cell neutral beams inject 2.5 MW of power for heating and beta studies. These experiments were carried out in the standard tandem-mirror operating mode rather than the thermal-barrier mode. At densities above 10^{12} cm^{-3}, the beam coupling to the low-energy ions increases, as indicated by the increase in $T_{i\parallel}$ shown in Fig. 5a. The average ion perpendicular energy for this

operation was 2 keV. The average plasma beta increases to 6% at higher density and is limited by beam power.

With 2-kV extraction, low-energy neutral injection (LENI), the ten injectors are designed to fuel the central-cell plasma at densities above 3×10^{12} cm^{-3} without gas fueling. Buildup calculations using the TREQ code predict that density buildup will require 170 atom amps incident and 10 ms particle confinement time. In the experiments to date, the incident LENI beam current and particle confinement time are each a factor of 2 to 3 less than these levels, except for periods shorter than the required 20-ms buildup time. As a consequence, the density of the trapped beam ions increases to only 4×10^{11} cm^{-3} with LENI beam injection. Thallium beam probe density measurements (Fig. 5b) and diamagnetic loop measurements (Fig. 5c) both indicate that this could be a promising method of fueling the plasma core with modest energy ions. The emphasis of our present work is to understand and improve confinement while increasing the LENI beam current so that a higher plasma density can be sustained with the LENI beam system.

A very important question for tandem mirrors concerns the electron temperature that can be achieved with open field line geometry. Central-cell electron temperatures have reached 290 eV. As shown in Fig. 6, this temperature can be strongly correlated with the stored end-cell diamagnetic energy. The achievement of these electron temperatures is significant because it indicates the absence of very strong electron power losses along open field lines.

4. AXIAL CONFINEMENT AND PLASMA POTENTIAL MEASUREMENTS

Past measurements of TMX-U axial plasma potential profiles were obtained during experiments with single-ended plugging. More recently we have developed several new methods using particle beam probing (described in Appendix A) to measure plasma potential in different axial locations with improved energy and temporal resolution and with redundancy. We conclude that thermal barriers as large as 0.75 kV are present in TMX-U.

We are currently carrying out measurements under various TMX-U operating conditions. An example of our recent thermal barrier region potential measurements is shown in Fig. 7. Figure 7a shows the thermal barrier potential measurements as a function of time. These are made by measuring the reflection energy of a 24° hydrogen pump beam with an end-loss ion spectrometer (ELIS) [6]. In this shot, the thermal-barrier depth reaches 0.75 kV at 44 ms. The PPC end plates are grounded in this operation. Note that the thermal-barrier depth rapidly decreases when the 2 ω_{ce} ECH is turned off. These measurements are localized along magnetic field lines as indicated by the pump neutral beam footprints shown in Fig. 7b. Using these footprints to estimate spatial locations of the potential measurements, we have constructed the axial potential profile shown in Fig. 7c. The solid circle is measured with a thallium ion-beam probe at z = 0. The solid square is from the centroid of the transmitted 6F-18° beam measurements and the open squares are from the energy spread in the transmitted signal assuming a monotonic decreasing potential. The solid diamond is from the centroid of the reflected 2A-24° pump beam and is arbitrarily located at the end-cell midplane. The barrier coulld be even deeper, since atoms ionized at that location would be trapped

and not detected. The open diamonds are obtained from the centroid of the transmitted signal and are plotted symmetrically around the potential minimum. The bar indicates the ELIS energy range between the minimum energy detected and the energy of the maximum current. The open triangle is the calculated potential that provides the measured 13-ms axial confinement time. The measured barrier depth is 0.75 kV, much larger than the ±0.1 kV uncertainties of this data.

5. CONCLUSIONS

Thermal-barrier experiments have been carried out in the TMX-U tandem-mirror experiment. Measurements of nonambipolar and ambipolar radial transport show that these processes, as well as end losses, can be controlled at modest densities and durations. Central-cell heating methods using ICH and neutral-beam injection have been demonstrated. Potential measurements with several recently developed methods indicate that deep (0.75 kV) thermal barriers can be established. These results provide encouragement to the prospect that the tandem mirror could be developed into an attractive reactor concept.

REFERENCES

1. T. C. Simonen et al., "Plasma Physics and Controlled Nuclear Fusion Research," in Proc. 10th Inter. Conf., London, England, 1984, IAEA, Vienna, 2 255 (1985).
2. D. P. Grubb et al., Phys. Rev. Lett. 53, 783 (1984).
3. E. B. Hooper et al., Phys. Fluids 27, 2264 (1984).
4. E. B. Hooper et al., Phys. Fluids 28, 3609 (1985).
5. S. Allen et al., Rev. Sci. Inst. 57, 2072 (1986).
6. J. H. Foote, Rev. Sci. Inst. 57, 1786 (1986).

APPENDIX A. NEW TMX-U THERMAL-BARRIER DIAGNOSTIC MEASUREMENTS

1. Plasma Potential Diagnostics

This appendix describes several of our new methods to measure plasma potentials at different axial locations of TMX-U. Table A-1 lists our various potential diagnostics, and Fig. A-1 indicates their spatial location.

The central-cell potential is measured with a thallium ion beam probe. We have also used a small ion energy analyzer inserted into the plasma to measure the plasma potential and cross calibrate the thallium beam probe. Both these diagnostics can make radial scans.

We employ several diagnostic methods in the thermal-barrier end cells to determine the axial potential structure. Here we have less spatial resolution than in the central cell. The end-loss ion spectrometer [1] (ELIS) and time of flight [2] (TOF) are discussed below. The turning-point microwave interferometer and the axial array of secondary emission charge exchange detectors are used to estimate the potential difference between the thermal-barrier midplane (where the sloshing beams are injected at 47° and 40°) and the location where they turn. These latter two diagnostics are semiquantitative, but both indicate that potential differences as large as 2 kV or more are present along field lines in the thermal-barrier region.

An ELIS at each end of TMX-U has proven to be an extremely powerful instrument to measure plasma potentials by measuring the energy distribution of the ions escaping on a given field line. Spatial localization is obtained with localized neutral gas puffing in the central cell or end plug, or is associated with pump neutral-beam injection in the end cell at the barrier midplane (24° pump beam) or between the central cell and the barrier midplane (18° pump beam). These beams inject ions into the magnetic loss cone that transit to the ELIS at the far end and arrive with an energy equal to their injection energy plus the plasma potential. Hydrogen pump beams are usually used in order to be distinguishable from the deuterium central-cell end losses. An example of the ELIS hydrogen spectra for the east and west ends is shown in Fig. A-2a and b. The variation in energy of the individual one-half and one-third energy components measures the plasma potential, and the width of the components measures the variation in potential within the beam footprint. Also shown in Fig. A-2b is a reflected component of beam 2A. The presence of this signal is a clear indication of a deep thermal barrier and/or large beta. The appearance of 1/18th energy components (associated with accelerated H_2^0) is also seen in Fig. A-2a and indicates that the plasma-confining potentials are less than $E_b/18 \sim 1$ kV at this time. The energy of the deuterium ions escaping from the central cell is a measure of the maximum potential. During strong end plugging, as indicated in Fig. A-2c and d, this signal is absent. In that case we have puffed gas near the outer potential peak to supply ions. To obtain sufficient signal, we needed to puff so much gas that the potential is reduced. Nevertheless we found that as the ion signal becomes detectable, the potential is slightly larger than that in the central cell; indicating an overall-ion confining potential and indicating an outside potential peak.

We are beginning to employ TOF charge exchange analyzers to examine the ion energy distribution in the thermal barrier

region. One analyzer views the east plug at 22.5° with respect to the magnetic axis and the other views the west plug at 3.4°. These viewing angles are within the magnetic-loss cone ($\theta_{LC} \approx 30°$), so the shape of the ion-distribution function is indicative of the thermal-barrier ion-confining potentials.

Figure 3a-c shows the spectra measured on the TOF analyzer during a period with good particle confinement, just before loss-of-plugging, and just after loss-of-plugging. While plugged, the TOF spectrum extends to energies above 0.9 keV. For deuterium ions, this indicates that the potential difference between the barrier and the plug exceeds 650 V. The TOF spectrum just before loss of plugging indicates a single Maxwellian distribution, suggesting that the barrier-trapped ions are in equilibrium with the passing ions; i.e., the barrier has filled in. We have modeled the ion distribution in the barrier using the multiregion Fokker-Planck code SMOKE, as shown in Fig. A-3a and b. After the loss of plugging, the breaks in the spectrum at 550 eV provide a possible measure of the potential difference between the inner mirror and the barrier. The ions confined in the barrier appear up to energies of 280 eV. The break at 280 eV is a possible measure of the potential difference between the barrier and the outer potential maximum. This potential is in agreement with the potential determined from the pump-beam measurement by the ELIS.

2. Hot Electron and Sloshing-Ion Diagnostic Measurements

During the initial operation of TMX-U, strong axial plugging was observed [3] only when the number of mirror-trapped electrons n_{mt} was a large fraction of the total thermal-barrier density n_T. At present, a twist-holographic reflector is employed for second harmonic thermal-barrier heating and a uniform slotted radiator for first harmonic potential peak production, and the ECH power has increased threefold. Now the hot electron distribution shown in Fig. 4a has two Maxwellian components: a warm ($\lesssim$50 keV) and a hot ($\gtrsim$70 keV) [4]. To evaluate the mirror-trapped fraction, two methods have been developed. The first is based primarily on x-ray diagnostics [4]. Figure 4b and c show results from the second method [5], which provides faster time resolution by using optically thin perpendicular electron-cyclotron emission. These measurements, which are model-dependent, suggest that 40 to 70% of the electrons are mirror-trapped.

Measurements of the sloshing ions during strong end plugging indicate that their lifetime may be shorter than that estimated from charge exchange and coulomb scattering, and that the density at the outside turning point is lower than would be expected unless the thermal-barrier depth exceeds about 2 kV. To investigate these anomalies we puffed D_2 gas into the end cell. With 1 TL/s injected near the turning point, the reduction in the sloshing-ion density was consistent with the bounce-averaged increase in end-cell neutral density. With higher gas injection (4 TL/s) into the thin-fan regions, the sloshing-ion lifetime was reduced by nearly a factor of three. Charge exchange analyzer data are shown in Fig. A-5. During the gas puff, the sloshing-ion energy distribution exhibits peaks associated with the full, half, and third energy beam components characteristic of a charge exchange-dominated plasma. Without

gas puffing, the energy distribution is smoother and has a significant component above the full injection energy, suggesting the presence of enhanced-velocity space-energy diffusion. For gas injection near the midplane, however, little effect on the sloshing ions was observed, indicating better neutral shielding, as expected.

APPENDIX REFERENCES

1. J. H. Foote, Rev. Sci. Inst. 57, 1786 (1986).

2. M. R. Carter, Bull. Am. Phys. Soc. 31, 1404 (1986).

3. R. A. James et al., Phys. Fluids 29, 2748 (1986).

4. E. H. Silver et al., submitted to Nucl. Fusion, "Plasma Diagnostic Techniques in Thermal-Barrier Tandem-Mirror Fusion Experiments," Lawrence Livermore National Laboratory, Livermore, CA, UCRL-95297 (1986).

5. R. A. James et al., Rev. Sci. Inst. 57, 1968 (1986).

Table A-1. TMX-U potential profile measurement methods.

Central Cell
Thallium ion beam probe
Ion energy analyzer
End Cell
End loss ion spectrometer (ELIS)
Standard ion end loss analysis
Gas puff at outer turning point
Pump beam ion transmission
Pump beam ion reflection
Pump beam energy spread
Pump beam 18th energy ion component
Time of Flight (TOF) charge exchange analyzer
East end 22.5° (in loss cone)
West end 3.4° (in loss cone)
Turning point microwave interferometer
Axial array of SED charge exchange detectors

FIGURE CAPTIONS

Figure 1. (a) Variation of radial average central-cell nonambipolar radial transport time with plasma potential shows agreement with neoclassical theory. (b) Thallium ion-beam probe measurements of the central-cell potential show a sharp decrease when the end walls are floated.

Figure 2. Measurements of (a) central-cell density and (b) ionization current I_e and total measured loss current I_T. These measurements show that TMX-U can operate with small ambipolar losses.

Figure 3. Thallium ion-beam probe central-cell radial profiles of (a) secondary current (proportional to $n_e \langle \sigma v \rangle$) and (b) plasma potential. At 22 ms the plasma is plugged, but with large ambipolar transport, and at 42 ms the plasma is not plugged and ambipolar transport is small.

Figure 4. (a) Measurements of ICRF heating with diamagnetic loop and end-loss spectrometer (ELIS). (b) Axial density profile during high-density plugging using ICRF.

Figure 5. Results of central-cell neutral-beam injection: (a) Using 20 kV beams without strong end plugging, we show average beta $\langle \beta \rangle$, parallel ion temperature $T_{\parallel}$, and diamagnetic energy confinement time τ_E as a function of on-axis electron density; (b) with 2-kV LENI beams, the thallium ion-beam probe measures a small, but encouraging, increase in density; while (c) the diamagnetic loop indicates an increase in the central-cell energy.

Figure 6. High central-cell electron temperature measured by Thomson scattering is correlated with end-cell diamagnetic energy (or ECH power).

Figure 7. (a) Simultaneous plasma potential measurements in the TMX-U thermal-barrier region, (b) axial locations of pump beam intersections with plasma and measured hot electron i/e diamagnetic length, and (c) axial potential profile constructed at 44 ms. The rise in the potential at 6.8 m is not measured directly by the ELIS but is indicated by the lack of density at the outer sloshing-ion turning point.

Fig. A-1. Spatial locations of plasma-potential diagnostics.

Fig. A-2. End-loss ion spectrometer data during potential measurements.

Fig. A-3. TOF charge-exchange energy spectra measured (a) with good total particle confinement, (b) just before loss of plugging, and (c) just after loss of plugging.

Fig. A-4. Measurements of hot electrons during strong plugging; (a) x-ray energy spectra, (b) ECE measurements of hot electron components compared to total density, and (c) hot electron temperature compared to diamagnetic energy.

Fig. A-5. Charge-exchange energy spectra of sloshing ions at a 40° pitch angle are shown for cases with and without gas injected near the thin fans. For the gas injected case, the full, half, and third energy-beam components are evident.

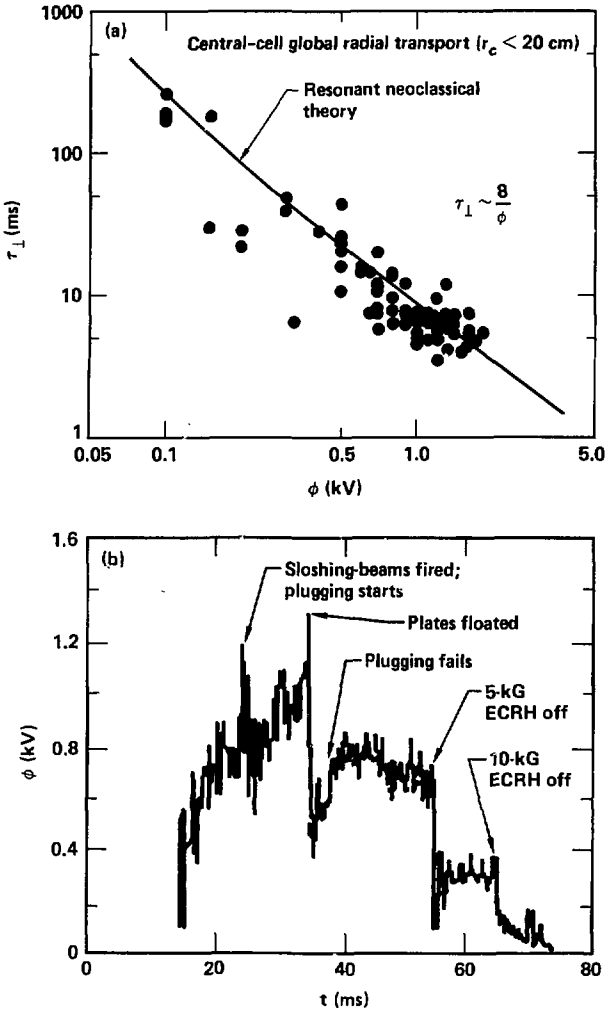

Figure 1. (a) Variation of radial average central-cell nonambipolar radial transport time with plasma potential shows agreement with neoclassical theory. (b) Thallium ion-beam probe measurements of the central-cell potential show a sharp decrease when the end walls are floated.

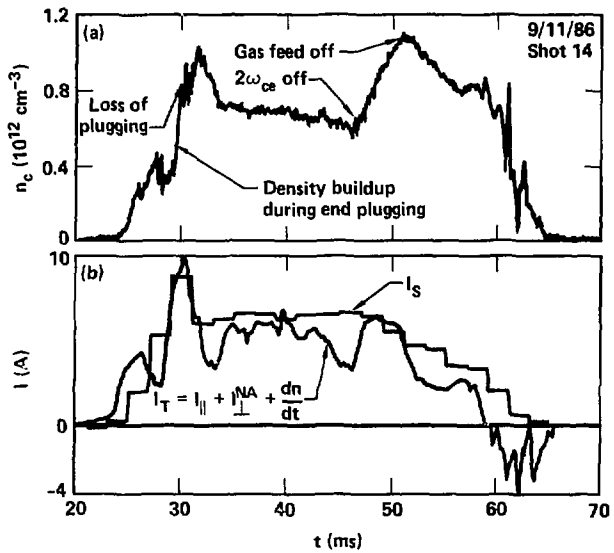

Figure 2. Measurements of (a) central-cell density and (b) ionization current I_s and total measured loss current I_T. These measurements show that TMX-U can operate with small ambipolar losses.

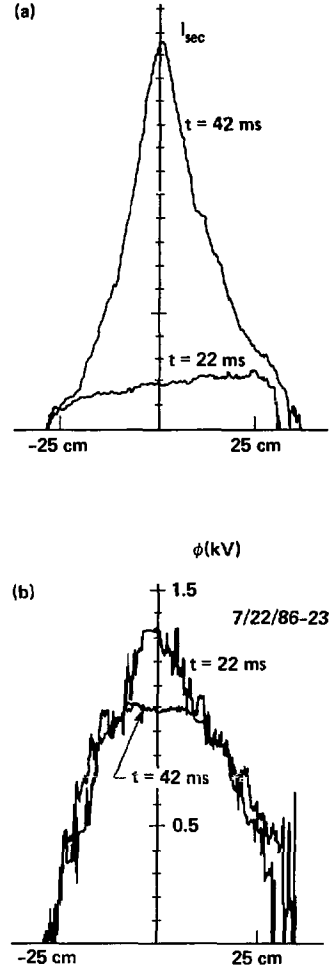

Figure 3. Thallium ion-beam probe central-cell radial profiles of (a) secondary current (proportional to $n_e \langle \sigma v \rangle$) and (b) plasma potential. At 22 ms the plasma is plugged, but with large ambipolar transport, and at 42 ms the plasma is not plugged and ambipolar transport is small.

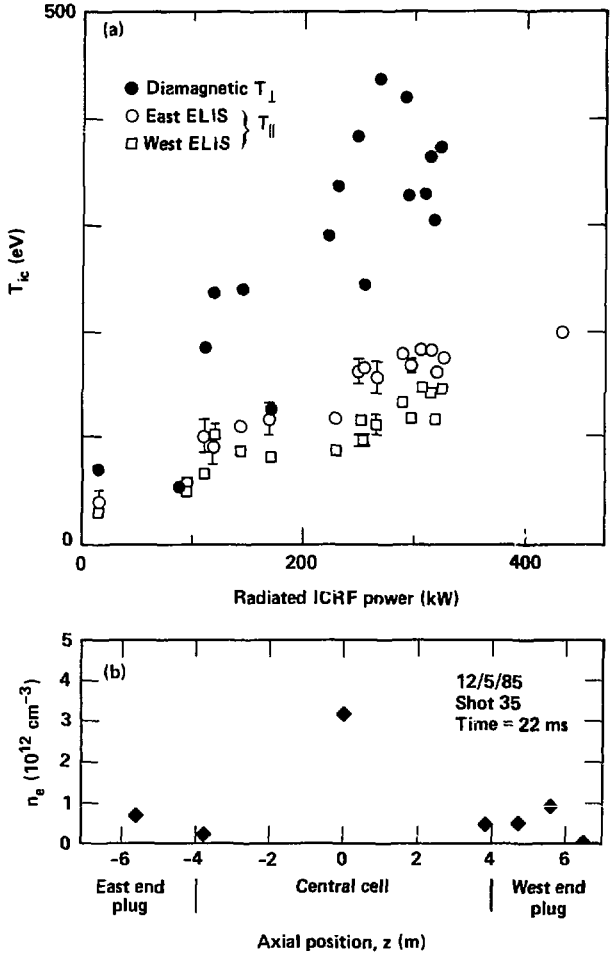

Figure 4. (a) Measurements of ICRF heating with diamagnetic loop and end-loss spectrometer (ELIS). (b) Axial density profile during high-density plugging using ICRF.

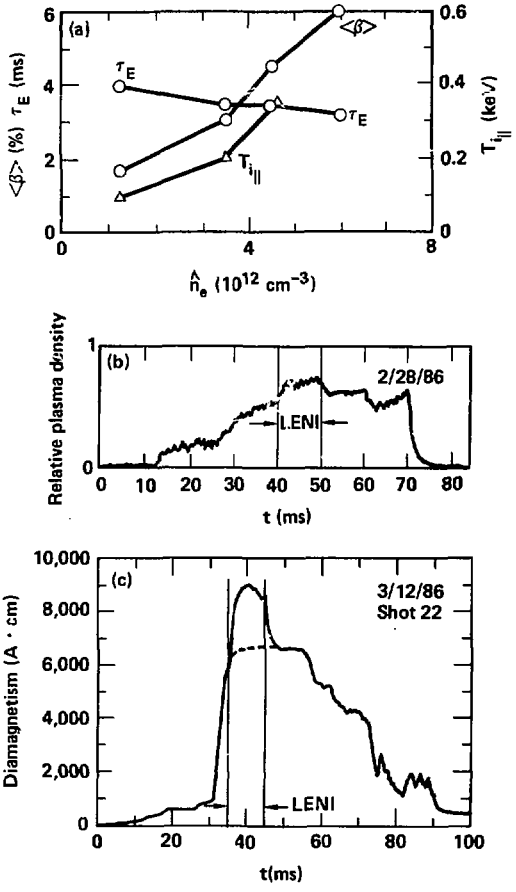

Figure 5. Results of central-cell neutral-beam injection: (a) Using 20 kV beams without strong end plugging, we show average beta <β>, parallel ion temperature $T_{i_{||}}$, and diamagnetic energy confinement time τ_E as a function of on-axis electron density; (b) with 2-kV LENI beams, the thallium ion-beam probe measures a small, but encouraging, increase in density; while (c) the diamagnetic loop indicates an increase in the central-cell energy.

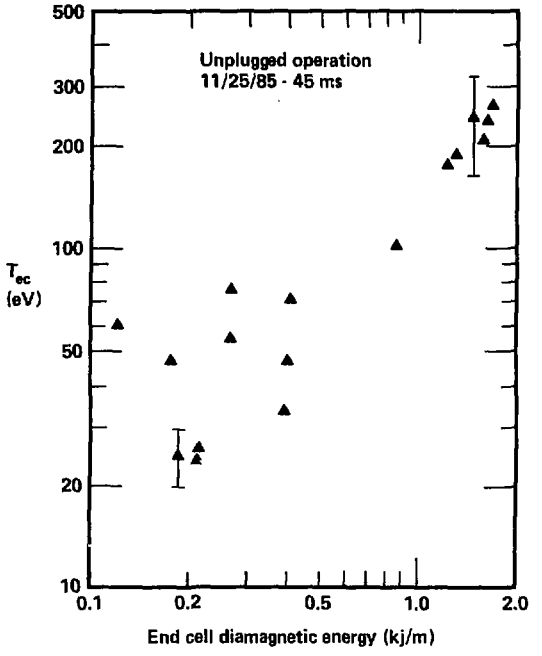

Figure 6. High central-cell electron temperature measured by Thomson scattering is correlated with end-cell diamagnetic energy (or ECH power).

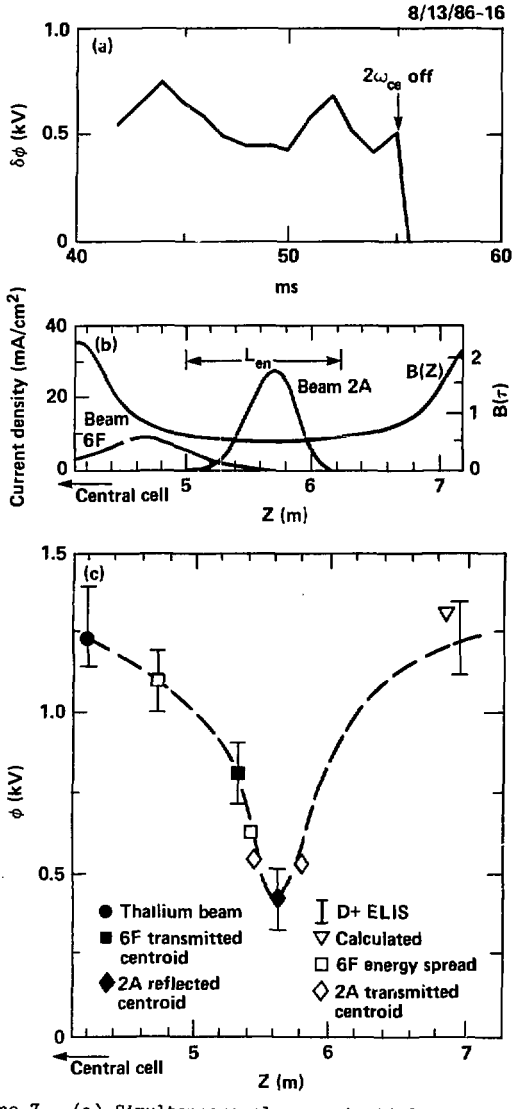

Figure 7. (a) Simultaneous plasma potential measurements in the TMX-U thermal-barrier region, (b) axial locations of pump beam intersections with plasma and measured hot electron 1/e diamagnetic length, and (c) axial potential profile constructed at 44 ms. The rise in the potential at 6.8 m is not measured directly by the ELIS but is indicated by the lack of density at the outer sloshing-ion turning point.

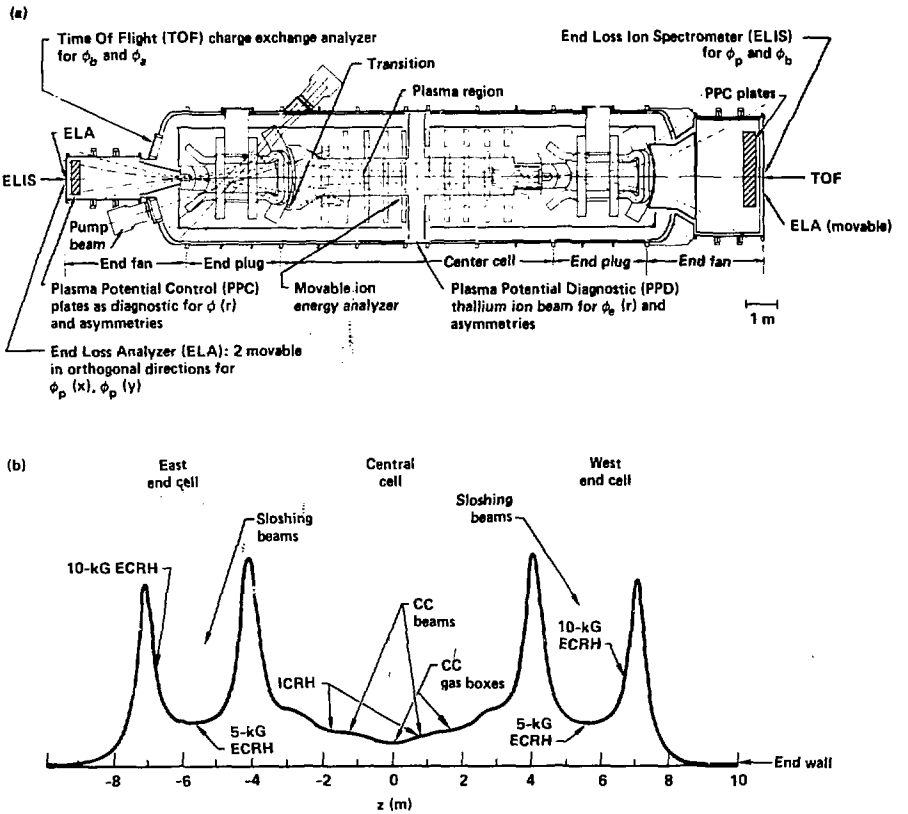

Fig. A-1. Spatial locations of plasma-potential diagnostics.

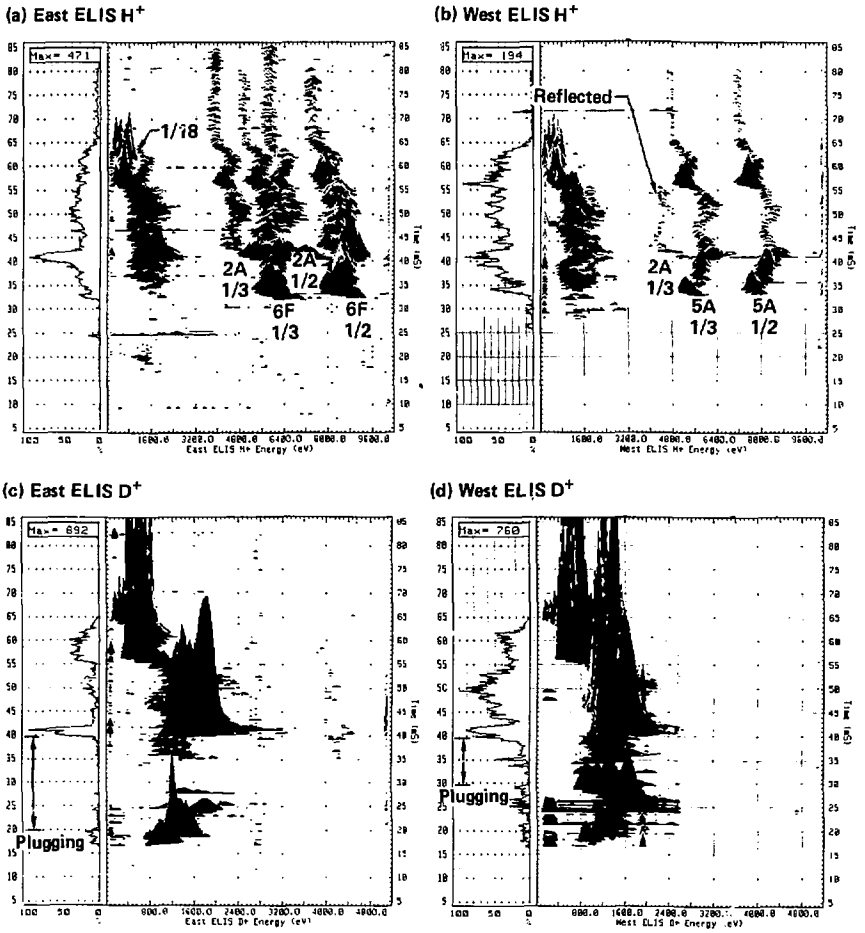

Fig. A-2. End-loss ion spectrometer data during potential measurements.

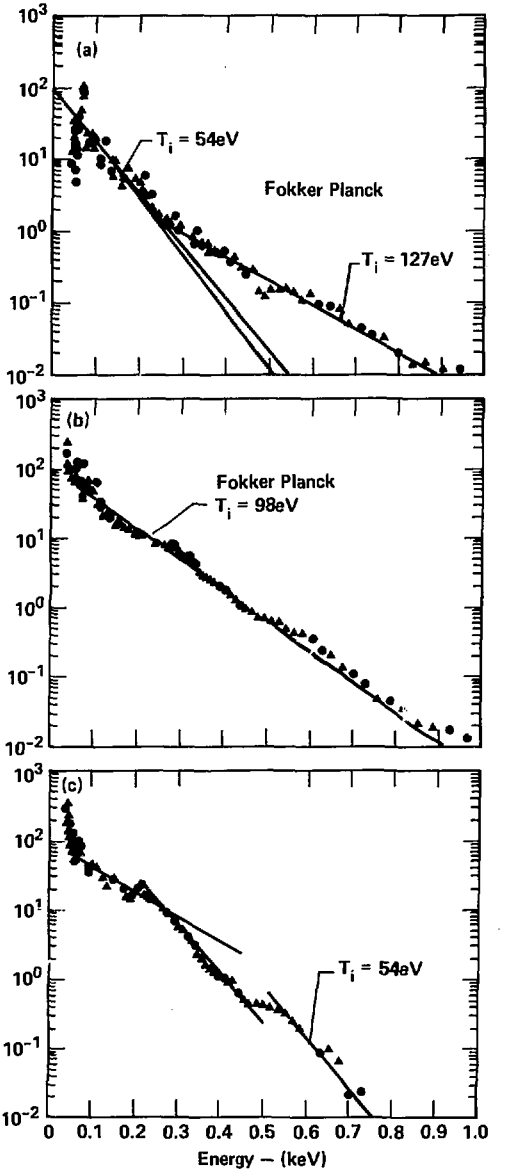

Fig. A-3. TOF charge-exchange energy spectra measured (a) with good total particle confinement, (b) just before loss of plugging, and (c) just after loss of plugging.

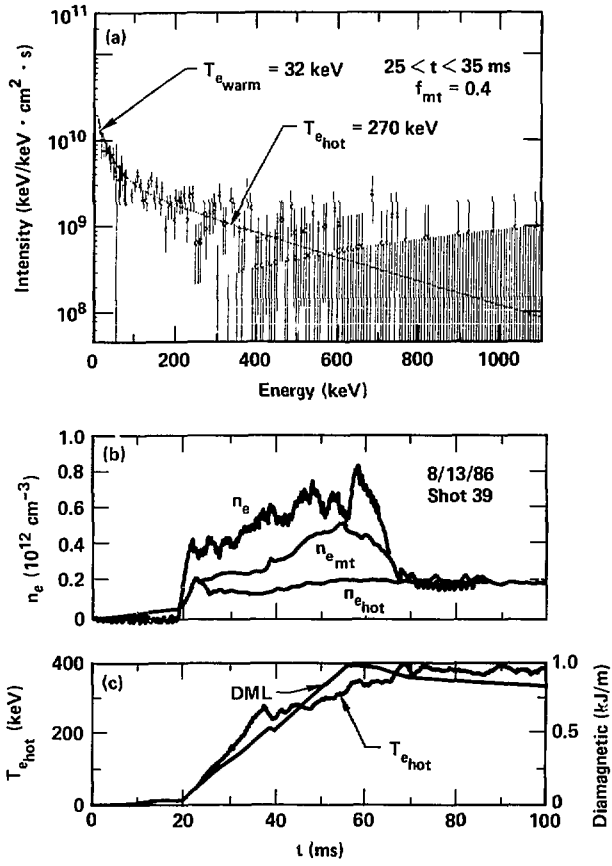

Fig. A-4. Measurements of hot electrons during strong plugging; (a) x-ray energy spectra, (b) ECE measurements of hot electron components compared to total density, and (c) hot electron temperature compared to diamagnetic energy.

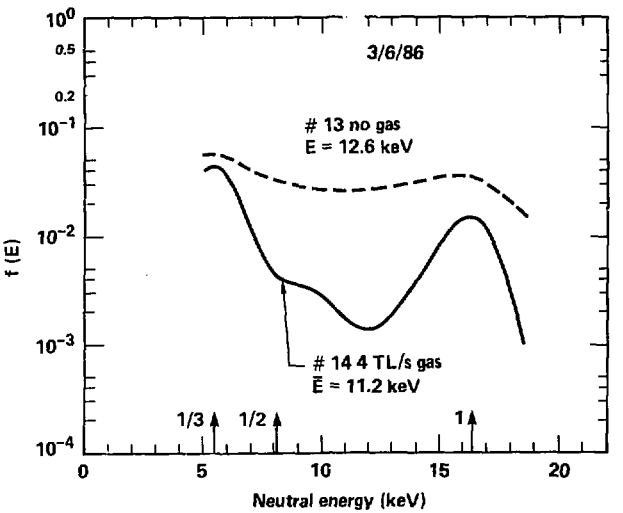

Fig. A-5. Charge-exchange energy spectra of sloshing ions at a 40° pitch angle are shown for cases with and without gas injected near the thin fans. For the gas injected case, the full, half, and third energy-beam components are evident.